令和 5年度　修士論文

Evaluation of Interfacial Thermal Resistance of Al-GFs Composite by Using Image-Based Calculation

指導教員　杉尾　健次郎　教授

広島大学大学院工学研究科　機械物理工学専攻

材料物理学研究室

M215113 LYU XINGYAO

ABSTRACT

With the development of equipment, devices with small volume and large heat generation continues to appear, and higher heat dissipation materials are required. carbon materials reinforced Al-matrix composites attract great interest from researchers of electron packaging materials due to their lightweight superior thermal properties. Especially for graphite flakes (GFs) reinforced Al-matrix composites, their excellent thermal properties, such as high thermal conductivity (TC) meeting the thermal performance requirements of electron packaging materials. The effective thermal conductivity (ETC) of graphite flakes (GFs)/Al composites is significantly influenced by the anisotropic thermal conductivity of GFs and the interfacial thermal resistance between both components. The Al powder of average diameter 30μm and graphite flake of average diameter 137 μm as reinforcement materials is used in this study. The as received powders are mixed for 5vol.%,10vol.%,15vol.%,20vol.% fraction of graphite in V-type ball milling process. The composites are fabricated by spark plasma sintering (SPS) method. The microstructures images of the composites were observed, and their relative density and ETCs were measured. And the average angles of the GFs with respect to the heat flow direction were calculated to be 18.6°, 16.3°, 14.6°, and 14.1°, respectively. A two-dimensional (2D) image-based simulation was used in this study to investigate the effect of both the orientation of GFs and interfacial thermal resistance on the ETC of the composite. The R values at the GFs/Al interface were evaluated to be 7.29×10^{-7}, 5.49×10^{-7}, 10×10^{-7}, and 12.15×10^{-7} W m^{-2} K^{-1} for Samples.

TABLE OF CONTENTS

LIST OF TABLES

CHASPTER 1 INTRODUTION

1.1 Overview

Now is the era of rapid development of electronic technology. As shown in Figure 1-1, abundant electronic products have entered people's daily life, making people's life more convenient, comfortable, and safe. Therefore, it is very necessary to ensure the efficiency, stability and safety of electronic products to people's lives.

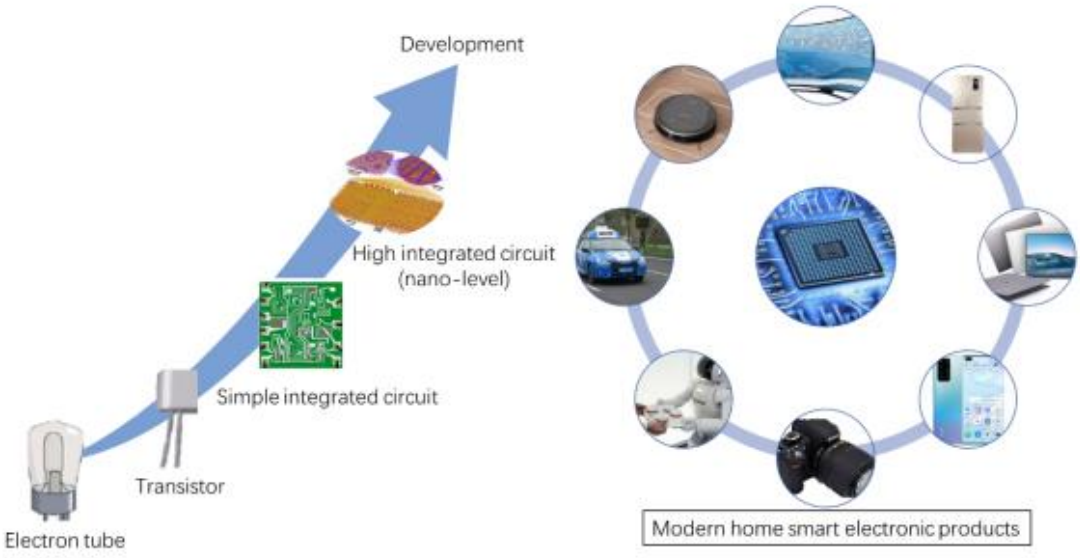

Figure1-1 The development of microelectronics and modern smart products.

However, with the rapid development of electronic technology in the direction of high energy, high frequency, and integration, heat generation per unit volume becomes very rapid. As a result, the generated heat will heat up the electronic components, which can seriously affect their working efficiency and life cycle, or even directly damage them if they cannot be dissipated in time[1]. In other words, if the heat conduction performance does not match the heat generation efficiency of electronic products, it will cause damage to electronic devices. The key to solving such problems is to develop

new heat-conducting materials, which have the characteristics of high heat-conducting performance.

Metal matrix composites not only have high thermal conductivity, but also easy processability and good plasticity. Therefore, they have attracted the attention of many researchers. Al is a matrix material with low density, low cost, high thermal conductivity and is widely used for the preparation of metal matrix composites.

It is fortunate that graphite flakes also have excellent thermal properties and are low-cost. Their TCs are values (~2200, ~38) W m^{-1} K^{-1} [2,3,4] in the basal-plane and the out-plane. In view of GFs excellent thermal properties, GFs/Al composites are one of the most promising candidates for electronic packaging.

Taking full advantage of the effective thermal conductivity (ETC) of graphite flakes-reinforced Al metal matrix composites, many experimental studies of the effective thermal conductivity (ETC) of GFs/Al composites have been conducted extensively.

it is crucial to study the effect of interfacial thermal resistance. In this study, GF/Al composites were prepared. To explore the effect of GF orientation and interfacial thermal resistance on the effective thermal conductivity (ETC) of GF/Al composites, a 2D image-based simulation method [5] was used to calculate the ETC value of GF/Al composites.

1.2 Research background

1.2.1 Traditional materials

Traditional electronic packaging materials include metals, ceramics, and composites. As shown in Table 1-1, the thermal conductivity of traditional electronic packaging materials. However, conventional materials such as copper, silver, gold, alumina, etc., have high density. As a result, they cannot meet the extensive development needs of electronic products, such as high integration, high-efficiency heat conduction, and green environmental protection.

Table 1-1 thermal properties of traditional electronic packaging materials.[6]

Materials	Density/g·cm^{-3}	TC/W·m^{-1}·K^{-1}
Al	2.7	236
Cu	8.9	400
Ag	10.49	429
Au	19.3	318
Al_2O_3	3.9	20
BeO	2.9	250-275
SiC	3.2	270
AlN	3.3-4.5	220

To meet the development characteristics of future electronic products, such as high integration and miniaturization of integrated circuits, portability, efficiency, high power, stability, and low cost, the next-generation electronic packaging materials need to possess the following properties.

1. High TC
2. Lower density
3. Sufficient strength
4. Cost control and competitive requirements

As the matrix of metal matrix composites, aluminum has low density, low cost, and high thermal conductivity, which can well meet these requirements. The reinforcement as a composite material mainly contains carbon materials(Carbon fiber, Graphite, Diamond), SiC, and Si. Table 1-2 shows their densities and thermal conductivities.

Table 1-2 Thermal properties of reinforcement [7,8,9]

Materials	Density/g·cm^{-3}	TC/W·m^{-1}·K^{-1}
Carbon fiber	1.75-2.19	530-1200
Graphite	2.23	- 3000(xy) 6-38(z)
Diamond	3.51	2500
SiC	3.2	270
Si	2.3	150
BeO	2.9	250

As shown in Table1-2, graphite flakes have extremely high thermal conductivity in the plane direction, and its density is relatively low compared to other materials. It is a very suitable reinforcement for aluminum-based metal composites.

1.2.2 Previous studies

Numerous experimental studies on the effective thermal conductivity (ETC) of GFs/Al composite materials have been conducted extensively,e.g,Chen et al.[10] reported that the ETC of 80vol.% GFs/Al composites(783W m^{-1}K^{-1}) was higher than that of 80vol.% diamond/copper composites[11](724wm-1k-1).Li et al [12] reported that the ETC of 70vol.% GFs/Al composite was 714wm^{-1}k^{-1} in the plane parallel to the GFs layers.

Compared to SiC/Al, Si/Al, Dimond/Al composite materials, GFs/Al composite materials demonstrate higher TC, lower cost, and better processability. However, the GFs/Al composite materials may not achieve the expected theoretical values due to the following three reasons:

A. Graphene flakes orientation: The orientation of graphene flakes in the composite material may be uneven. Inconsistent orientation of graphene flakes can disrupt the heat conduction path, leading to reduced thermal conductivity.

B. Interface thermal resistance: There is an interface between the graphene flakes and aluminum in the composite material, which increases thermal resistance. The presence of this interface restricts heat transfer, thus affecting the thermal conductivity of the composite material.

C. Interface reactions: During the fabrication process of GFs/Al composites, interface reactions can occur easily, leading to the formation of Al_4C_3 at the GFs-Al interface. Unfortunately, Al_4C_3 is a brittle compound that has detrimental effects on the composites. It reduces the plasticity of the material and accelerates fatigue crack growth rates.

In previous studies, several theoretical models have been proposed to predict the effective thermal conductivity (ETC) of composites. However, these theoretical models are not suitable for calculating the ETC of GFs/Al composites due to the diverse orientation of the GFs within the composites.

Additionally, to evaluate the interfacial thermal resistance at the GFs-Al interface, commonly used methods include the phonon diffuse mismatch model (DMM) [13], acoustic mismatch model (AMM) [14], and others. However, these models assume of an ideal interface to calculate interfacial thermal resistance. The microstructure of the contact interface between two solids is extremely complex and influenced by various factors, such as thermophysical properties, hardness, shape, roughness of the materials, the gap at the interface, and more. Moreover, it is highly challenging to establish a direct relationship between these influencing factors and the contact interface microstructure. As a result, the existing models have inherent limitations in accurately calculating the interface thermal resistance. Due to this complexity and lack of a clear correlation, these models may not be entirely reliable for evaluating interfacial thermal resistance in

practical scenarios. As a result, further research and development are necessary to improve the accuracy of predicting interfacial thermal resistance in GFs/Al composites and similar materials.

1.3 research purpose

To fully utilize the high thermal conductivity (TC) of GFs and maximize the effective thermal conductivity (ETC) of GFs/Al composites, it is essential to explore the impact of anisotropic TC and interfacial thermal resistance. In this study, different content GFs/Al composites were prepared, and the objective was to study the influence of GF orientations and evaluate interfacial thermal resistance on the ETC of the composites, a 2D image-based simulation method was employed to calculate the ETC of GF/Al composites.

CHAPTER 2 EXPERIMENTAL METHODS

2.1 Raw materials

The raw materials used in this study were aluminum (Al) powders and highly crystalline graphene flakes (GFs). The Al powders were obtained from the Institute of High Purity Chemistry in Japan, while the highly crystalline GFs were provided by Ito Graphite Industry Co., Ltd., also located in Japan.

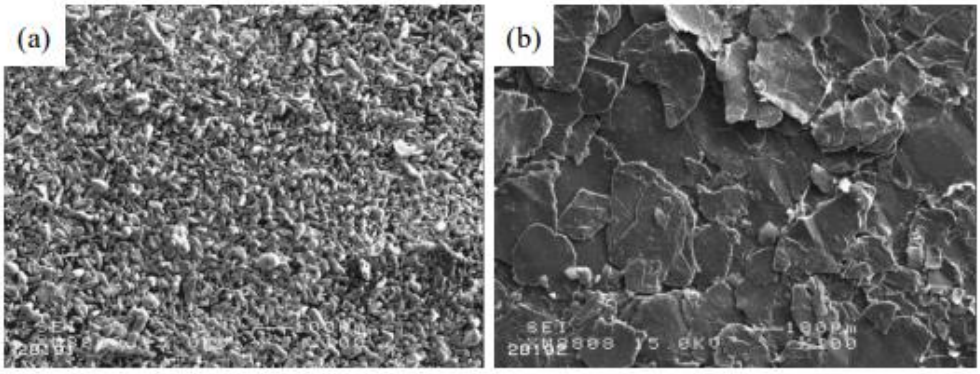

Figure2-1 Microstructures of raw materials: (a) Al powder and (b) GFs.

Figure 2-1 displays the microstructure of the Al powder and GFs. The Al powders exhibit a rugby-shaped morphology with uneven sizes, whereas the GFs have a flat surface with uniform thickness.

Table 2-1 Chemical components of Al and GFs.

Material	Carbon	Ash	Volatile	H_2O	Al	Cu	Fe	Si
				%				
Al								
GFs(XD150)	98.78	0.61	0.61	0.27				

Table 2-1 presents the chemical components of the raw materials. The Al powder boasts an impressive purity level of 99.9%, while the GFs have a purity of 98.8%. The high crystallinity of the GFs is expected to impede any chemical reactions between the Al and GFs. Furthermore, Table 2-2 provides information on some physical properties and thermal conductivity of both the Al powder and GFs.

Table 2-2 Shape and physical properties of Al and GFs.

Materials	Shape	d	ρ	C_p	TC
		μm	$g \cdot cm^{-3}$	$J \cdot kg^{-1} \cdot K^{-1}$	$W \cdot m^{-1} \cdot K^{-1}$
Al	powder	30	2.7	880	236
GFs	flake	137.02	2.23	710	880(in-plane) 38(out-plane)

2.2 Preparation of graphite flakes and Al powders mixtures

The wet mixing process was employed to blend Al powders and GFs in this study. Initially, the Al powders, GFs, and alumina balls were placed inside an aluminum jar. The mixtures were then mixed for a duration of 2 hours using a V-type mixer at a rotation speed of 50 rpm. Following the mixing step, the mixtures were dried in a constant temperature oven at 70 ℃. The mixing procedure of the raw materials, Al powder, and GFs, is illustrated in Figure 2-2.

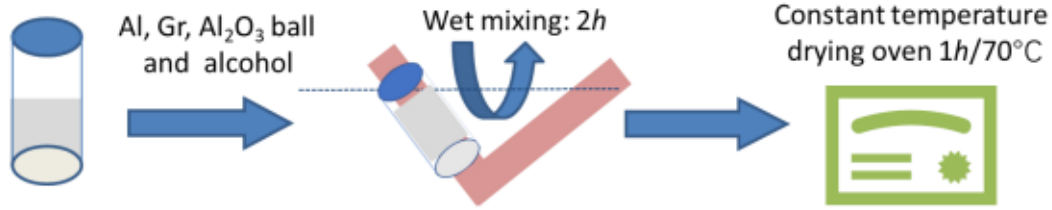

Figure2-2 Flowchart of GFs and Al powder mixing.

2. 3 Fabrication of graphite flakes/Al composites by sparking plasma sintering

Figure 2-3 shows the equipment of SPS. The mixed powders were filled into graphite molds (graphite molds) to prepare GFs/Al composites. The GFs were layered in the mixture by tapping the mold during the filling of the mixed powder. Subsequently, spark plasma sintering (SPS) was performed at a temperature of 873 K and a pressure of 60 MPa for 30 minutes under vacuum conditions. Sintering temperature was kept below the melting point of Al to prevent the reaction between Al and GFs. A pure Al sample was fabricated by SPS under the same condition as those composites. The cylindrical diameter and height of the samples are 10mm and 20mm. Table xx indicates the specific graphite flake content of the samples

Table2-3 Composition of the sample and its size and shape

Matrix(Vol%)	Reinforcement(Vol%)	Diameter(mm)	Height(mm)
100%Al	0%GFs	10	20
95% Al	5%GFs	10	20
90% Al	10%GFs	10	20
85% Al	15%GFs	10	20
80% Al	20%GFs	10	20

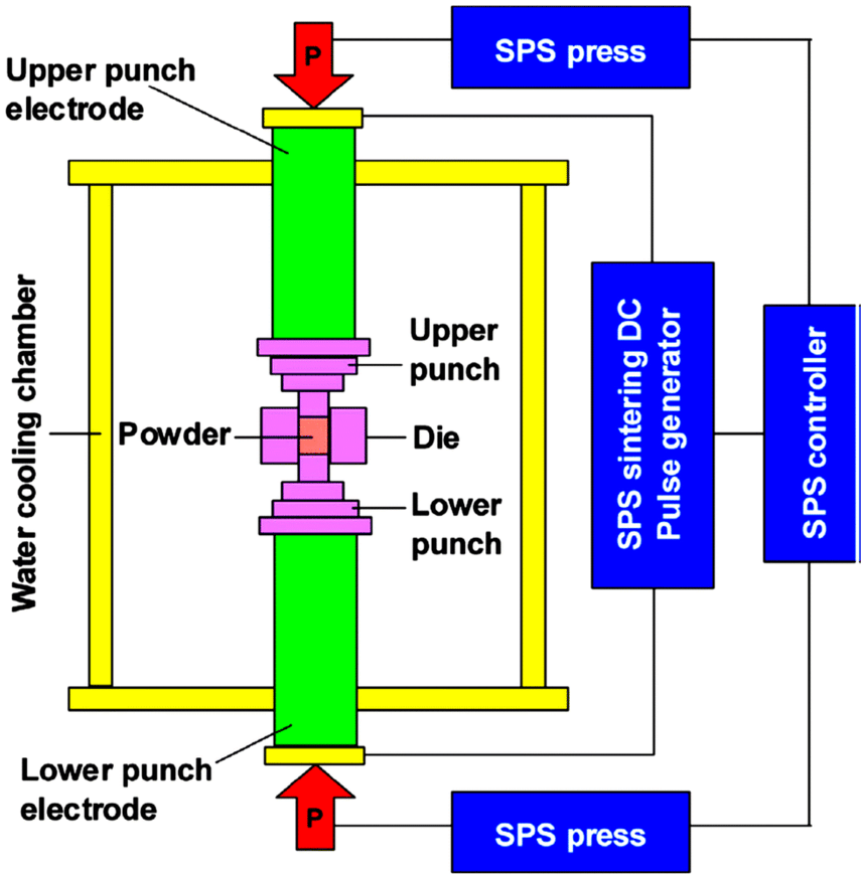

Figure 2-3 Schematic of the SPS equipment.

2.4 Relative density measurement

The relative density of the sample, is calculated by Archimedes' principle:

$$\rho = \frac{m_1}{m_1 - m_2} \tag{2.4.1}$$

m_1 in the equation represents the mass of the sample in air and m_2 represents the mass of the sample in water. The relative density is calculated from the following equation:

$$\rho_r = \frac{\rho}{\rho_t} \tag{2.4.2}$$

The microstructure of the sintered composites was observed by optical microscopy to understand the distribution of carbon fibers in the matrix. The orientation of the carbon fiber is then calculated from the metallographic photographs taken.

2.5 Microstructure observation

The Scanning Electron Microscope (SEM) utilizes a beam of electrons that is directed onto the solid surface or powder particles to generate different signals and produce an image. The primary purpose of SEM is to observe the morphology and structure of powders and fabricated composites.

To conduct SEM, the die containing the sample is fixed onto carbon tape, and the powder sample is applied and spread over the carbon tape. The prepared die is then placed inside the SEM chamber. Subsequently, the chamber is evacuated to create a vacuum. The electron beam is focused onto the surface of the sample, which results in the generation of various signals. These signals are then used to create a 2D image that provides valuable information about the surface morphology and microstructure of the materials under observation.

SEM is an indispensable tool in materials science and other fields where detailed imaging and analysis of surfaces and microstructures are required. It enables researchers to gain insights into the fine details of materials and provides a deeper understanding of their properties and characteristics.

2.6 Measurement of angle of the reinforcements in the matrix

The angle of the reinforcements in the composites is measured using scanned electron microscopic (SEM) images. The SEM images of the composites are processed using MPImage, an image-based analysis tool. During this analysis, the graphite flake reinforcements dispersed within the main matrix are enclosed within rectangles. These rectangles represent the orientation of the graphite particles. The angle between the basal plane of the graphite, which corresponds to the longer side of the rectangle, and the direction of heat flow is measured as the angle of the graphite flakes. Figure 2-4

illustrates the schematic representation of the angle measurement and how the graphite flakes are enclosed by the rectangle. These measured angles are then plotted against their relative frequency to visualize the distribution of the reinforcements within the metal matrix.

In summary, SEM images are used to determine the angles of the graphite flake reinforcements in the composites. These angles are obtained by enclosing the graphite particles within rectangles and measuring the angle between the basal plane of the graphite and the heat flow direction. The resulting data is then plotted to visualize the distribution of the reinforcements within the metal matrix.

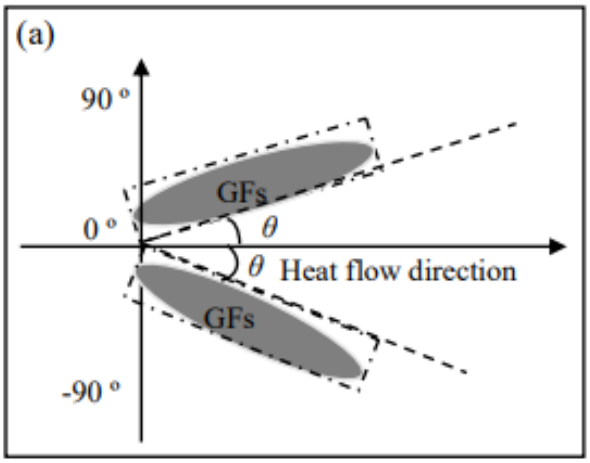

Figure 2-4 Schematic representation of the measurement of the angle

2.7 Thermal conductivity of GFs

This study used an angle (θ) between the basal plane of GFs and the direction of heat flow to characterize the GFs'orientation in composites. Thus, by using the following equation (2.7.1),(2.7.2) [15], the TC of GFs can be calculated along the direction of the basal plane of GFs parallel ($\lambda_{//}$) and perpendicular ($\lambda_{\perp}$) to the heat flow direction.

$$\lambda_{//} = \lambda_a \left[1 - \left(1 - \frac{\lambda_c}{\lambda_a}\right) sin^2\theta\right] \quad (2.7.1)$$

$$\lambda_{\perp} = \lambda_a \left[1 - \left(1 - \frac{\lambda_C}{\lambda_a}\right) cos^2\theta\right] \quad (2.7.2)$$

where λ_a and λ_c are the TC in the basal-plane and the out-of-plane directions of GFs, respectively. It can be observed that TC decreased significantly from 880 to 38 W m^{-1} K^{-1} when the angle increased from 0° to 90°, revealing that the orientation of the GFs significantly, illustrates the relationship between the TC of GFs and the angle θ.

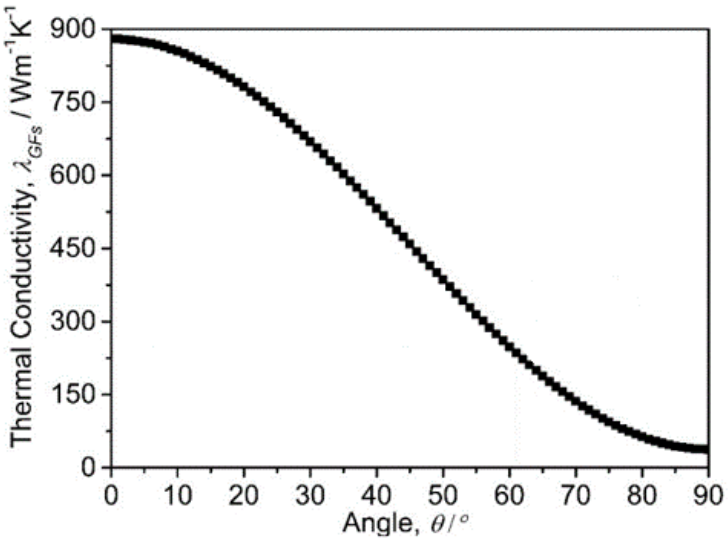

Figure 2-5 Effect thermal conductivity through heat flux direction with varied graphite angles.

2.8 Thermal conductivity measurement by experimental method

The method of thermal conductivity measurement depicted in Figure 2-6 is widely used due to its simplicity and cost-effectiveness. The schematic illustrates the measurement device for steady-state thermal conductivity.

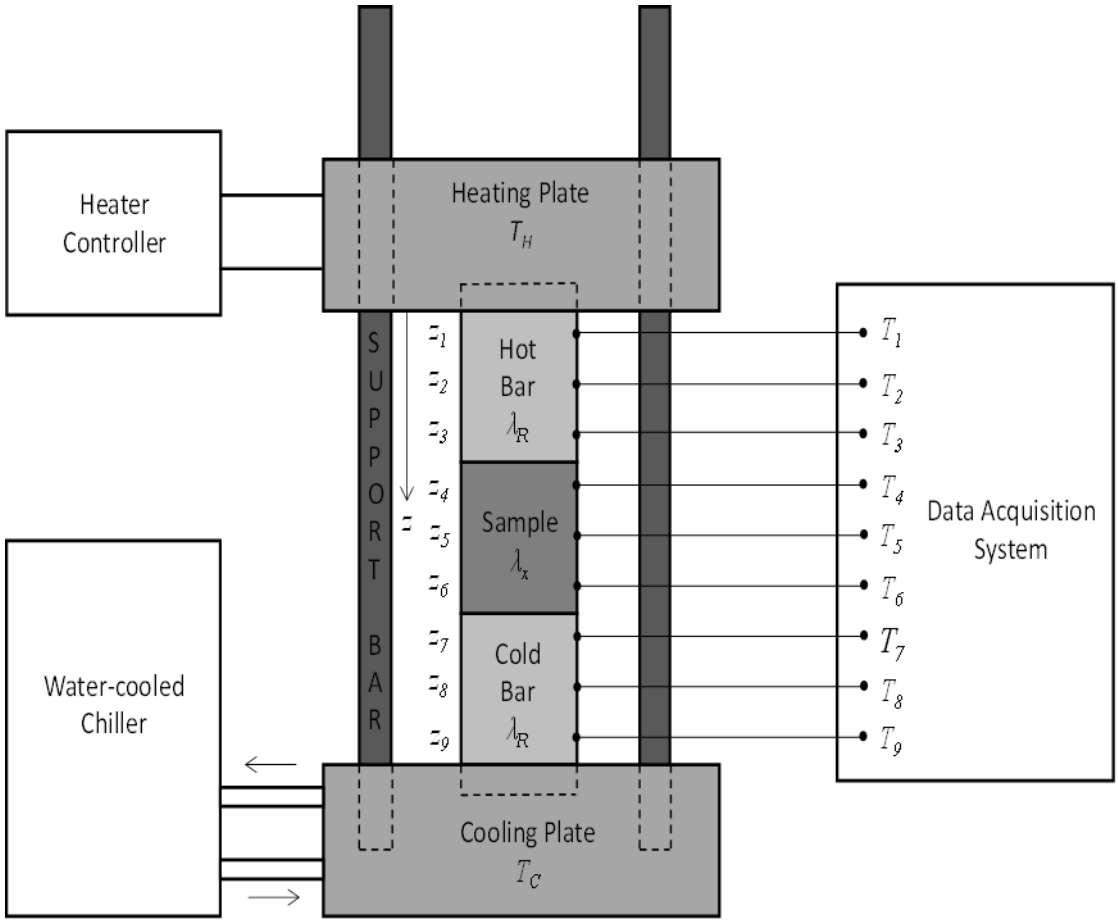

Figure 2-6 Schematic diagram of the steady-state thermal conductivity measurement device

To create a temperature difference, a hot plate above and a cold plate below are set up. In this experiment, the temperature of the hot plate was set to room temperature +5 °C and the temperature of the cold plate was set to room temperature -5 °C. The sample is clamped by a copper hot bar and a cold bar, both of which with 10 mm in diameter and 30 mm in length.

$$a_h = \sum_{i=1}^{3}(z_i - \bar{z}_h)(T_i - \bar{T}_h) \Big/ \sum_{i=1}^{3}(z_i - \bar{z}_h)^2\,, \quad \bar{z}_h = \frac{1}{3}\sum_{i=1}^{3} z_i\,, \quad \bar{T}_h = \frac{1}{3}\sum_{i=1}^{3} T_i \quad (2.8.1)$$

$$a_c = \sum_{i=7}^{9}(z_i - \bar{z}_c)(T_i - \bar{T}_c) \Big/ \sum_{i=7}^{9}(z_i - \bar{z}_c)^2\,, \quad \bar{z}_c = \frac{1}{3}\sum_{i=7}^{9} z_i\,, \quad \bar{T}_c = \frac{1}{3}\sum_{i=7}^{9} T_i \quad (2.8.2)$$

$$a_s = \sum_{i=4}^{6}(z_i - \bar{z}_s)(T_i - \bar{T}_s) \Big/ \sum_{i=4}^{6}(z_i - \bar{z}_s)^2\,, \quad \bar{z}_s = \frac{1}{3}\sum_{i=4}^{6} z_i\,, \quad \bar{T}_s = \frac{1}{3}\sum_{i=4}^{6} T_i \quad (2.8.3)$$

where Z_i is the distance between the *i*-th thermocouple and the heating plate, and T_i is the temperature of the *i*-th thermocouple. Finally, the effective thermal conductivity of the sample (λ_{eff}) can be calculated by fowling equation;

$$\lambda_{eff} = \frac{\lambda_{Cu} C(\Delta T_h + \Delta T_c)}{2\Delta T_s} \quad (2.8.4)$$

where λ_{Cu} is the thermal conductivity of copper bar (λ_{Cu} = 385 $Wm^{-1}K^{-1}$); *C* is a correction factor, and it is a constant value (i.e., *C* = 236/257).

2.9. Thermal conductivity evaluated by 2D image-based simulation method

The finite volume method was used to calculate the two-dimensional temperature distribution. The temperature of an element can be calculated using the following equation:

$$T_{x,y}^{n+1} = T_{x,y}^{n} + \frac{\Delta t}{\rho c}\left(\frac{q_{x+1,y}^{n} - q_{x-1,y}^{n}}{\Delta x} + \frac{q_{x,y+1}^{n} - q_{x,y-1}^{n}}{\Delta y}\right) \quad (2.9.1)$$

where $T_{x,y}^{n}$is the temperature of the element at (x, y) coordinates, $T_{x,y}^{n+1}$ is the temperature of the element at (x, y) coordinates after a time Δt, ρ is the density, c is the specific heat, and Δx and Δy are the sizes of the elements. The heat flow q^ncan be calculated as follows:

$$q_{x+1,y}^{n} = \lambda\left(\frac{T_{x+1,y}^{n} - T_{x,y}^{n}}{\Delta x}\right),\ q_{x-1,y}^{n} = \lambda\left(\frac{T_{x,y}^{n} - T_{x-1,y}^{n}}{\Delta x}\right)$$
$$q_{x,y+1}^{n} = \lambda\left(\frac{T_{x,y+1}^{n} - T_{x,y}^{n}}{\Delta y}\right),\ q_{x,y-1}^{n} = \lambda\left(\frac{T_{x,y}^{n} - T_{x,y-1}^{n}}{\Delta y}\right) \quad (2.9.2)$$

When the heat flow q^nmove at the GFs-Al interface:

$$q^n_{x+1,y} = h(T^n_{x+1,y} - T^n_{x,y}), q^n_{x-1,y} = h(T^n_{x,y} - T^n_{x-1,y})$$
$$q^n_{x,y+1} = h(T^n_{x,y+1} - T^n_{x,y}), q^n_{x,y-1} = h(T^n_{x,y} - T^n_{x,y-1}) \quad (2.9.3)$$

where h is the interfacial thermal conductance between different materials.

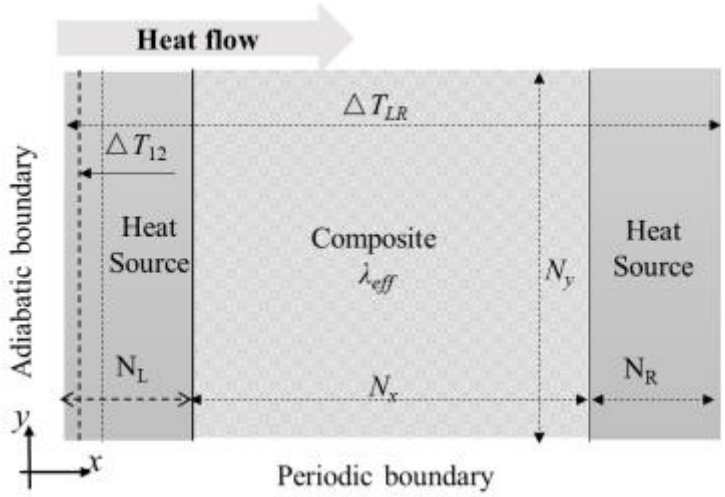

Figure 2-7 Simulation model for the ETC calculation.

Figure 2-7 shows the simulation model. It's a sandwich structure with two heat sources and a composite part. The composite part was obtained from the microstructure image of GFs/Al composites. The composite part had a size of 450x600 elements, and each heat source had a size of 5x600 elements (NL = NR = 5 elements). Each element size was 1.18×10^{-6} m.

The upper and lower sides had periodic boundaries, while the left and right sides were adiabatic boundaries. The temperatures of the left and right edge elements were fixed at 301 K and 300 K, respectively. The initial temperature of other elements was set to 300K. The temperature was iteratively updated until the variation was less than 10^{-13}K, reaching a steady-state temperature distribution. The effective thermal conductivity (ETC) of the GFs/Al composite, $\lambda_{eff,}$ was then calculated as follows:

$$\lambda_{eff} = \frac{\lambda_{Al} \Delta T_{12} N_x}{\Delta T_{LR} - N_L \Delta T_{12} - N_R \Delta T_{12}} \quad (2.9.4)$$

where λ_{Al} is the TC of the Al matrix, ΔT_{12} is the average value of the temperature difference between the first and second columns, and N_L, N_R, N_x are the number of elements along the corresponding direction.

2.10 Interfacial thermal resistance

Due to the different crystal structures of graphene fibers (GFs), it may have different thermal conductivity properties in the in-plane and perpendicular planes. Therefore, we calculated the thermal conductivity of the aluminum-GFs interface using the DMM method, referred to as the interfacial thermal conductivity *h*. The method for calculating h is as follows:

$$h = \frac{\hbar^2}{8\pi^2 K T^2} \sum_j \left[\frac{1}{v_{1,j}^2 v_{2,j}^2 \left(v_{1,j}^{-2} + v_{2,j}^{-2}\right)} v_{1,j} \int_0^{\omega_{1,j}^c} \frac{\omega^4 e^{\frac{\hbar\omega}{KT}}}{\left(e^{\frac{\hbar\omega}{KT}} - 1\right)^2} d\omega \right] \tag{2.10.1}$$

where $\hbar$ is Planck's constant, K is Boltzmann constant, T is temperature, ω is phonon angular frequency, and $\omega_{1,j}^c$ is the maximum phone angular frequency. The phono sound velocity, v, can be written as:

$$\sum_j v_j = v_L + 2v_r \tag{2.10.2}$$

$$v_L = \sqrt{\frac{E}{\rho}} \cdot \frac{1-\mu}{(1+\mu)(1-2\mu)} \tag{2.10.3}$$

$$v_T = \sqrt{\frac{E}{\rho}} \cdot \frac{1}{2(1+\mu)} \tag{2.10.4}$$

where v_L is longitudinal sound velocity, v_T is transverse sound velocity, E is Young's modulus, ρ is density, μ Poisson's ratio. The maximum phone angular frequency is calculated:

$$\omega_{1,j}^c = v_{1,j} \left(6\pi^2 \frac{\rho_1 N_A}{M_1}\right)^{\frac{1}{3}} \tag{2.10.5}$$

where N_A is Avogadro constant, M_1 is relative molecular mass. The material parameters are given in Table 3-4.

CHASPTER 3 RESULTS AND DISCUSSION

3.1 Prepared samples

Figure 3-1 shows the images of the prepared samples.

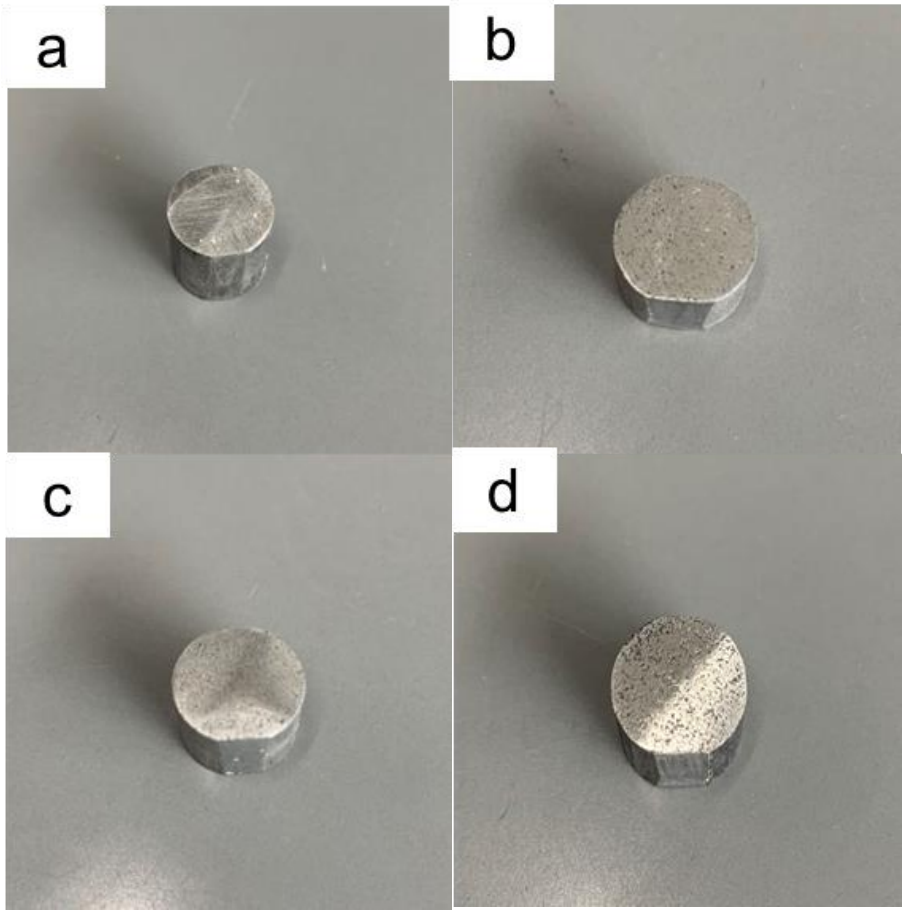

Figure 3-1 images of the prepared samples of 5 vol.% GFs/Al composite (a), 10 vol.% GFs/Al composite (b), 15 vol.% GFs/Al composite (c), 20 vol.% GFs/Al composite (d).

3.2 Microstructure characterization

Figure 3-2 shows the microstructure images of the mixtures of Al and 5-20 vol.% GFs. GFs were evenly dispersed in the Al powders, and GFs in Figure 3-2 (a-d) have the same particle size.

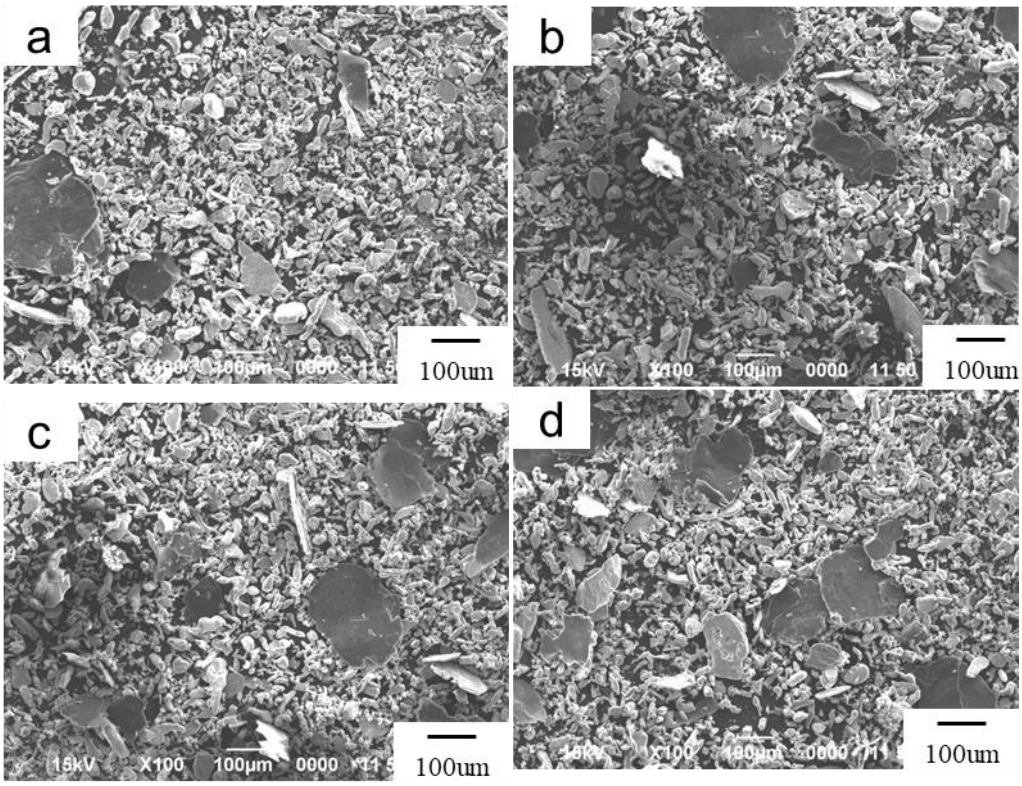

Figure 3-2 SEM images of the mixtures of Al and 5-20 vol. % GFs. 5 vol.% GFs (a), 10 vol.% GFs (b), 15 vol.% GFs (c), and 20 vol.% GFs (d).

SPS was used to prepare composites with 10-40 vol. % GFs/Al, as well as a pure Al sample. The relative densities of these materials were all above 98%, except for the pure Al sample, which had a relative density of 97%. The high relative densities indicate that the GFs/Al composites were effectively densified. Detailed values of the relative densities can be found in Table 3-1.

Table 3-1 Relative density of GFs/Al composites.

Sample	Pure Al	GFs/Al composites			
content	0	5vol.%	10vol.%	15vol.%	20vol.%
Relative density	97.0%	97.5%	98.8%	98.5%	98%

Figure 3-3 illustrates the shape of the samples sintered using SPS. The black arrows indicate that the C-plane the pressure during sintering. As a result, the GFs in the Al-matrix were stacked in layers, with the basal plane of GFs parallel to the C surface.

To observe the orientation of GFs in the Al-matrix more clearly, SEM images of the GFs/Al composites were taken from the A surface.

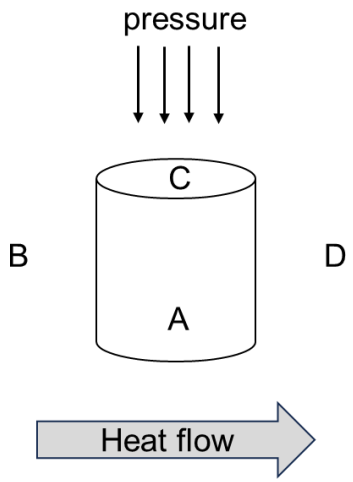

Figure 3-3 Schematic of the GFs/Al composites sintered by SPS. The grey arrow indicates that the heat flow was from B to D when measuring the ETC of the sample.

Figure 3-3 shows SEM images of GFs/Al composites with different amounts of GFs, ranging from 5% to 20%. In these pictures, the grey parts are aluminum, and the dark regions are the GFs. The GFs are evenly distributed throughout the aluminum and arranged in layers, just as we expected. Most of the GFs with the direction of heat flow, but a few GFs are oriented at an angle to the heat flow direction.

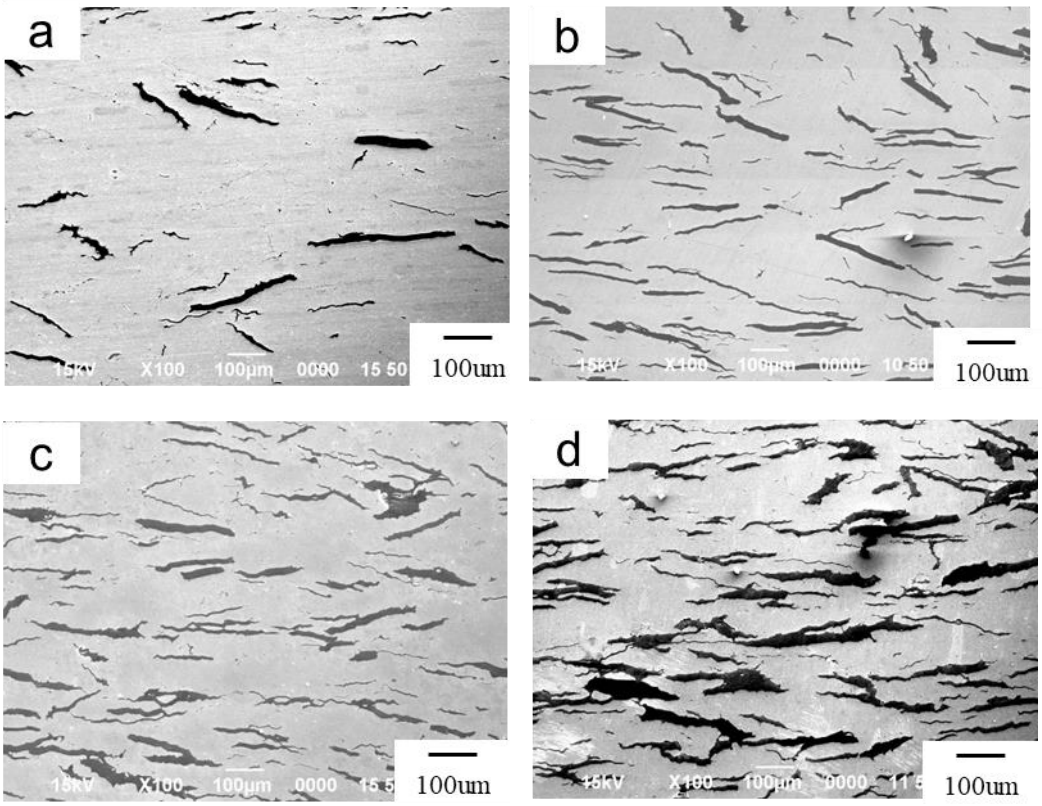

Figure 3-4 SEM images of 5-20 vol.% GFs/Al composites.

3.3 Effective thermal conductivity

The effective thermal conductivities of 5-20 vol. % GFs/Al composites and the pure Al sample were measured using a steady-state thermal conductivity measuring device (refer to Figure 2-6). Figure 3-5 (a-e) shows the temperature variation in the ETC measurement process.

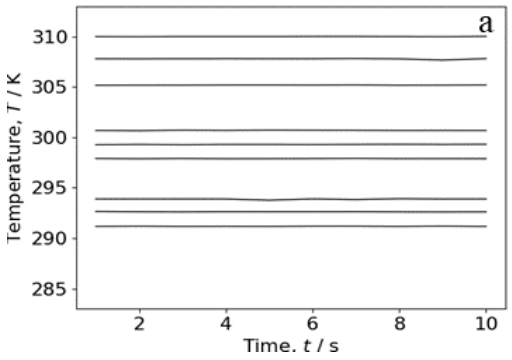
a
Temperature, T / K
Time, t / s

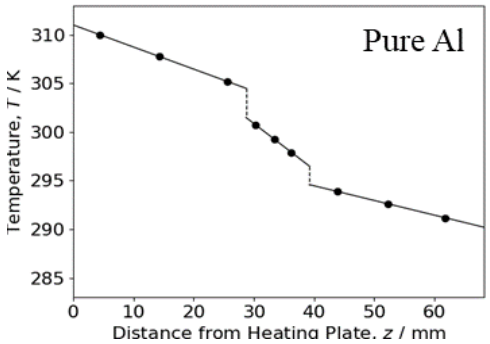
Pure Al
Temperature, T / K
Distance from Heating Plate, z / mm

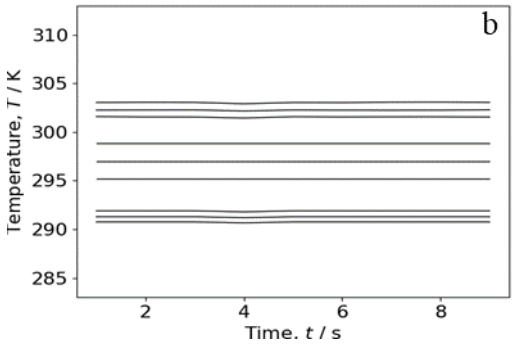
b
Temperature, T / K
Time, t / s

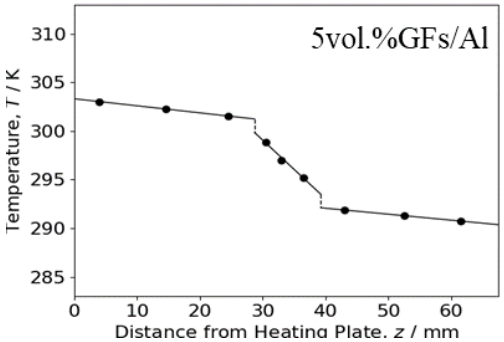
5vol.%GFs/Al
Temperature, T / K
Distance from Heating Plate, z / mm

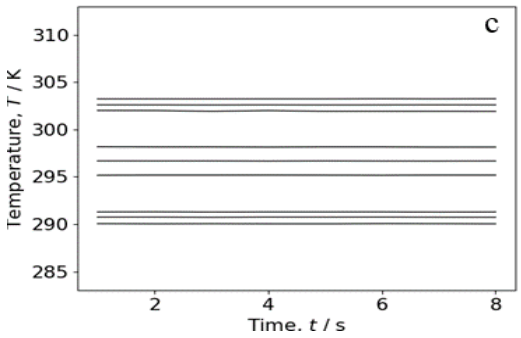
c
Temperature, T / K
Time, t / s

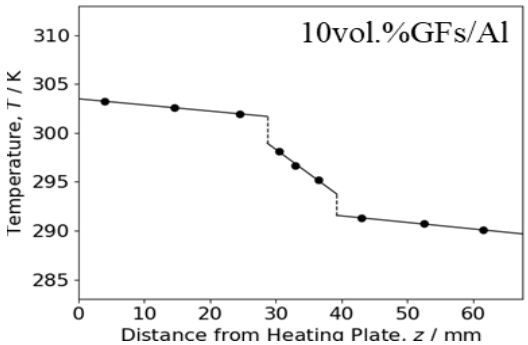
10vol.%GFs/Al
Temperature, T / K
Distance from Heating Plate, z / mm

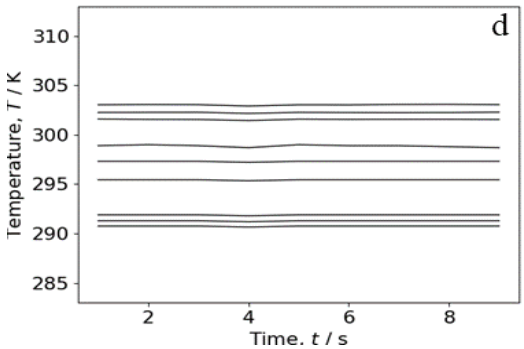
d
Temperature, T / K
Time, t / s

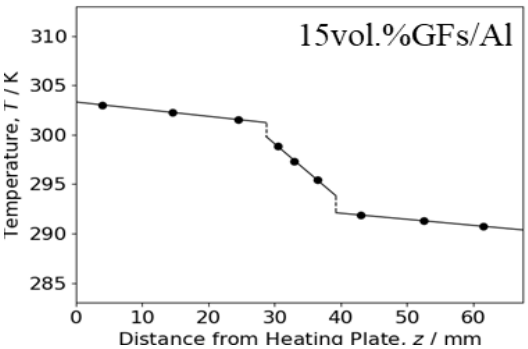
15vol.%GFs/Al
Temperature, T / K
Distance from Heating Plate, z / mm

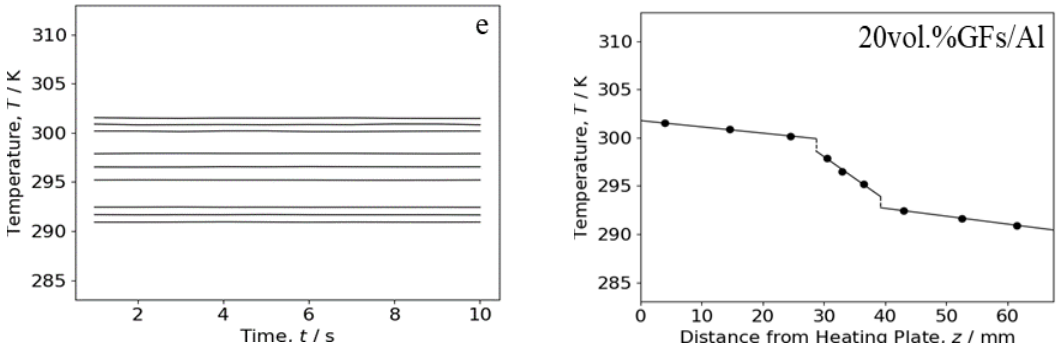

Figure3-5 Temperature variation in the ETC measurement process of 5,10,15,20vol.%GFs/Al composites, (a-e) relationship between temperature and time, relationship between temperature and distance of the measuring points.

3.4 Analysis of GFs orientations

An angle between GFs basal plane and heat flow direction was used to characterize the orientation of GFs in composites. The angle of the reinforcements is measure from the scanned electron microscopic (SEM) images of the composites. Figure 2.7.1shows the SEM images of the composites are processed in MPImage.an image-based analysis. And the average angle was counted through the software, as shown in Figure 3-6,and the results are presented in table 3-2. The thermal conductivity of the GFs was also recalculated through the equation(2.7.1),(2.7.2).

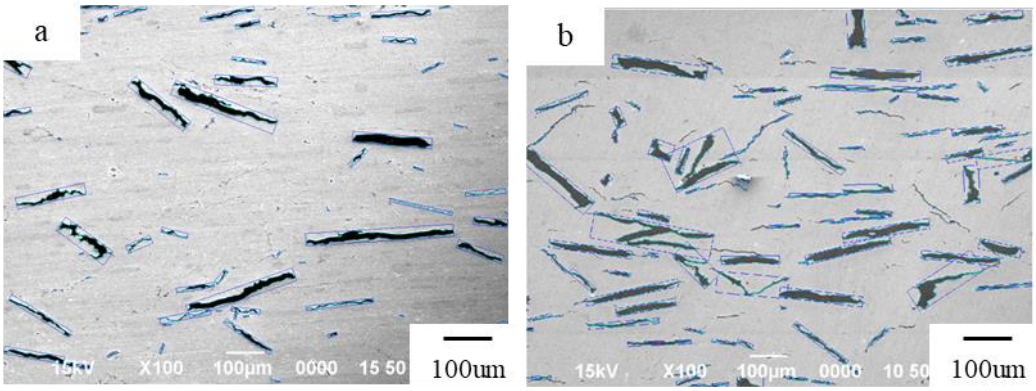

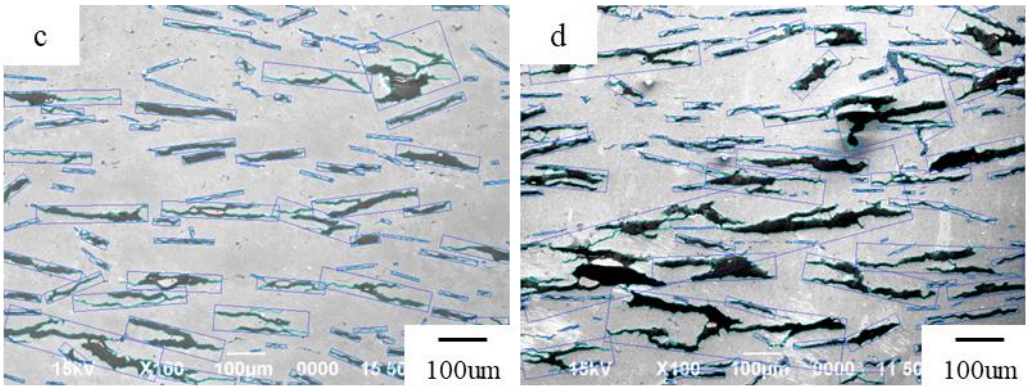

Figure 3-6 MPimage processed Analysis of GFs orientations.

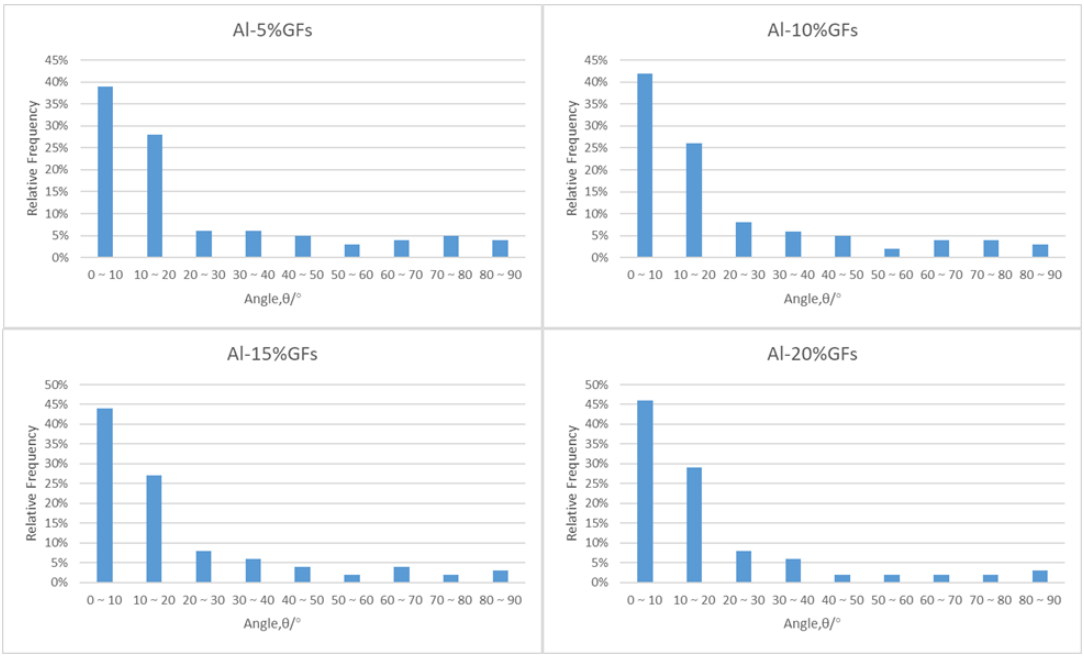

Figure 3-7 Distribution of GFs' orientation in the 5-20 vol.% GFs/Al composites, the orientation was described by the angle between GFs basal-plane direction and heat flow direction.

Table3-2 The average angle of GFs/Al composite and TC of GFs

sample	Al-5%GFs	Al-10%GFs	Al-15%GFs	Al-20%GFs
Average angle/°	18.6°	16.3°	14.6°	14.1°
TC of GFs/ $Wm^{-1}K^{-1}$	794.34	813.26	826.50	830.02

3.5Thermal Conductivity Correction

The measured relative density (as shown in Table3-3) indicated the presence of pores in the composites. Therefore, in this study, it is assumed that the pores of all the samples are located in the aluminum matrix and the effect of pores on the thermal conductivity is eliminated by using the following equation：

$$\lambda_{Al_{eff}} = \frac{1}{4}\left[\begin{array}{c}\lambda_p(3v_p-1)+\lambda_{Al}(3v_{Al}-1)+\\ \left(\left[\lambda_p(3v_p-1)+\lambda_{Al}(3v_{Al}-1)\right]^2+8\lambda_p\lambda_{Al}\right)^{\frac{1}{2}}\end{array}\right] \tag{3.5.1}$$

3.6 Simulation Result

3.5.1 Simulation ETC values of the composite

The ETCs (λ_{ROM}) of Samples 1–4 were calculated using the rule of mixture (ROM), i.e., $\lambda_{ROM} = (v_{GFs})(\lambda_{GFs}) + (1-v_{GFs})(\lambda_{Al\text{-}eff})$, where the value of GFs is the revised value by the equation(2.7.1),(2.7.2).The TC of the GFs (λ_{GFs}) was set to 794.34,813.26,826.50,830.02$Wm^{-1}K^{-1}$. The values of λ_{ROM} were 185.73,218.33,254.62, and 288.96 W m^{-1} K^{-1} for Samples 1–4, respectively. The calculated apparent thermal conductivity (λ_{ROM}) was significantly higher than the measured effective thermal conductivity (ETC). Additionally, we conducted 2D image-based simulations to verify the impact of GFs orientation on the effective thermal conductivity of the composites. And the values are listed in table 3-3

Table3-3 Calculation parameters and calculated effective thermal conductivities of composites.

sample	v_{Al}	v_p	λ_p	λ_{Al}	$\lambda_{Al\text{-}eff}$	λ_{ROM}	$\lambda_{s\text{-}eff}$
			W m^{-1} K^{-1}				
Al	0.97	0.03	0.214	160.8	153.7		
1	0.992	0.008			167.8	185.73	180.77
2	0.994	0.006			169.6	218.33	214.49
3	0.98	0.02			170.4	254.62	235.76
4	0.993	0.007			171.2	288.96	259.27

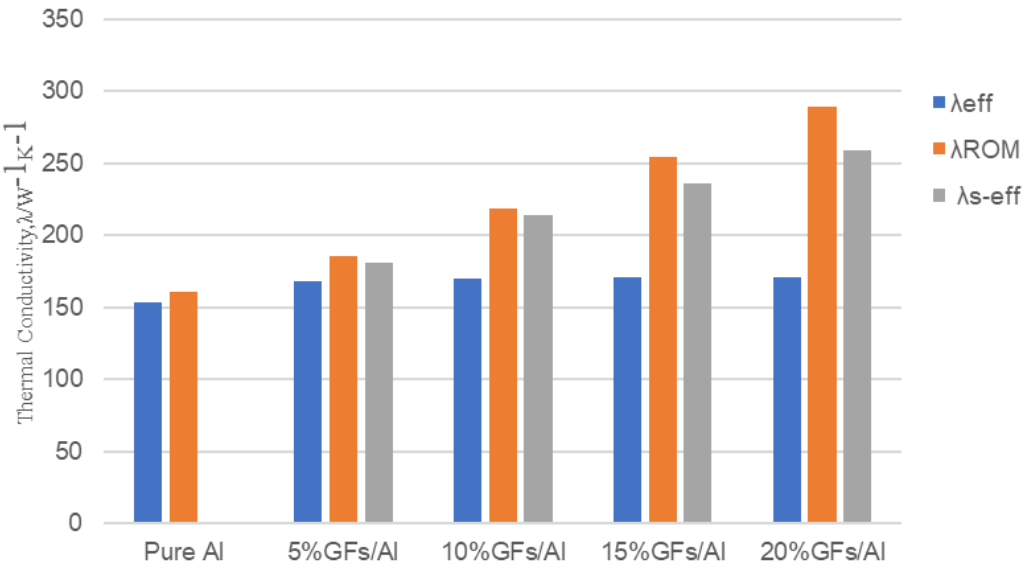

Figure 3-8 ETCs of the composite samples. λ_{eff} denotes the measured ETC, λ_{ROM} is the ETC calculated using the rule of mixture, and λ_{s-eff} is the ETC calculated using the 2Dimage-based simulation considering GF orientations.

3.5.2 Effect of the orientation of GFs on the effective thermal conductivity

The thermal conductivity (TC) values of GFs in the experimental samples were determined using equation (4-5), and the results were illustrated in Figure 3-9. GFs were represented by different colors based on their orientations within the Al matrix.

When the orientation of GFs was parallel to the heat flow direction, GFs exhibited high thermal conductivity and were marked in red.

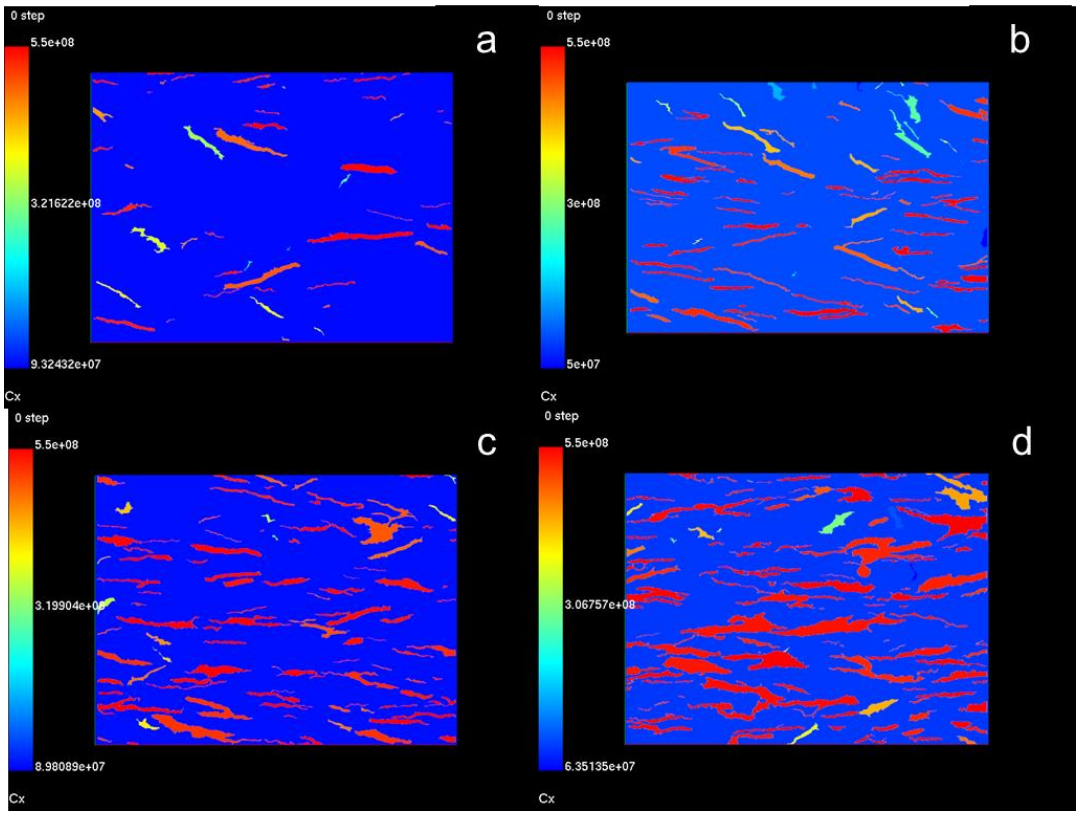

Figure 3-9 TC distribution values of GFs in Samples a-d. The color bar shows the TCs of GFs in different orientations; The red arrow indicates the heat flow direction.

3.5.3 Effect of interfacial thermal resistance on the effective thermal conductivity

A series of 2D image-based simulations were performed to study further the effect of the interfacial thermal resistance on the ETC of the composites. The heat transfer coefficient, h, ranged from $10^3$to 10^9 W m^{-2} K^{-1}at the Al–GF interface. Set the values of the h, ranged from $10^3$to 10^9 W m^{-2} K^{-1}at the Al–GF interface ,enter the values into the equations for the simulation, and derive the seven values of the ETC, and then plot these seven points as a one-line curve, as shown in Figure 3-10 ,illustrating ETC values as a function of h for composites.

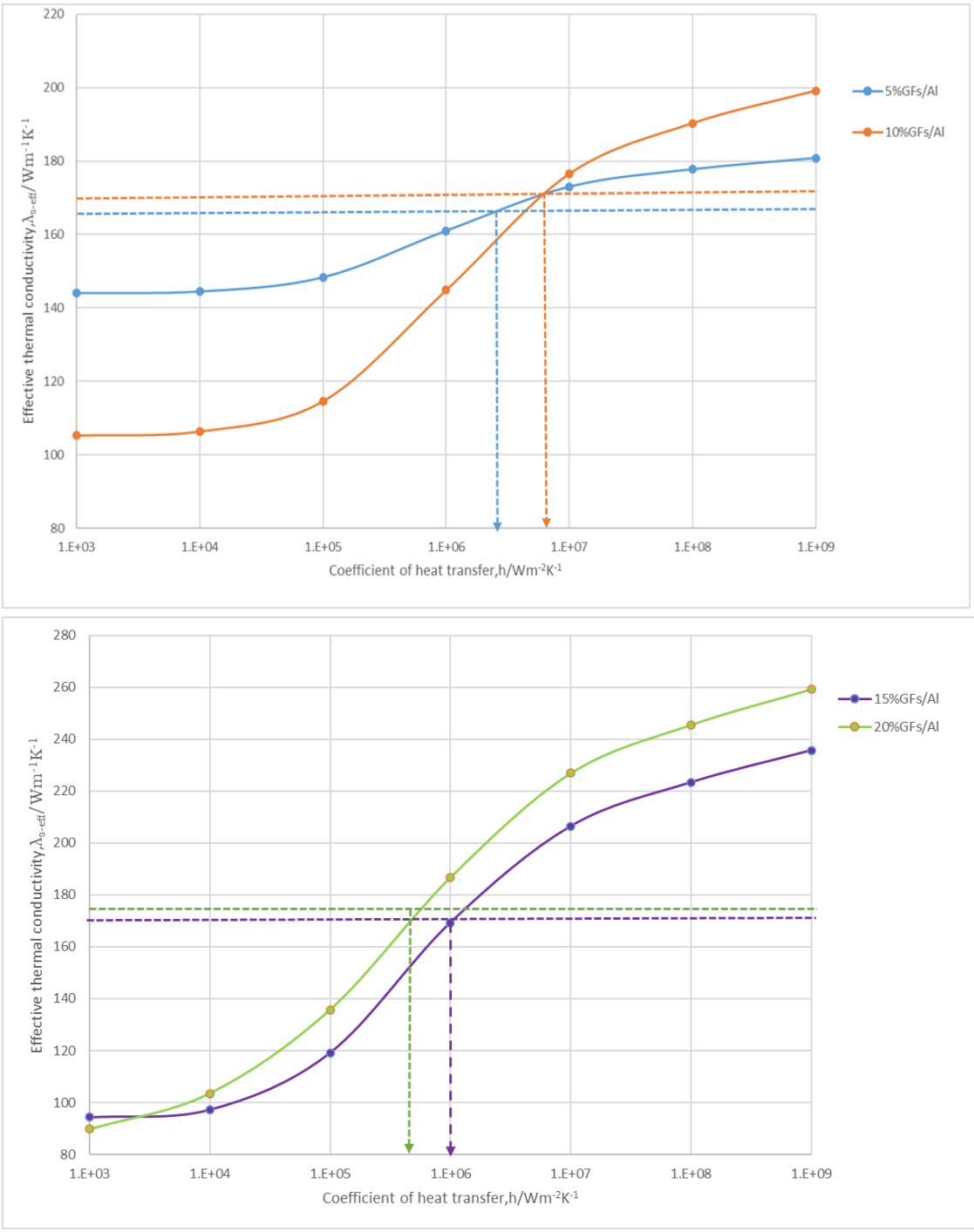

Figure 3-10 ETC as a function of the heat transfer coefficient, h. The dashed lines represent the experimental ETCs and the arrows denote the h value at the Al-GF interface.

The effective thermal conductivity (ETC) curve resembled the KJMA [36] equation, with ETC values showing a rapid increase as the heat transfer coefficients h

increased from 10^5 to 10^9. In Figure 3-10, the dashed lines represented the experimental ETC values, while the arrows indicated the heat transfer coefficients h at the Al-GF interface.

Table 4-3 presented the evaluated h values obtained through curve. The values showed a consistent order of magnitude for all samples, approximately 10^6. Additionally, Table 4-3 included a reference value of h calculated using the AMM model. The order of magnitude of the reference value is 10^7.And the values of h calculated by DMM were 1.1×10^8 $Wm^{-2}K^{-1}$ in the in-plane and 1.32×10^9 $Wm^{-2}K^{-1}$ in the out-of-plane. Thus, the values were greater than the simulated h. The interfacial thermal resistance, R, is the reciprocal of heat transfer coefficient, i.e., R = 1 / h, R values for Samples a–d were listed in Table 4-3.Their values decrease and then increase with the graphite flake content, probably because when the graphite flake content is low, the sample has more pores, and when the content becomes high, the sample has more cracks resulting in a larger interfacial thermal resistance for both.

Table3-4 Material parameters of the DMM calculation [17], interfacial thermal conductance (h), and interfacial thermal resistance (R); Sim. is the simulated h using 2D-image, Cal. is calculated h using DMM method, Ref. is the reference value of h.

Sample		T (K)	E (GPa)	P (g/cm^3)	μ	M1	h/10^6 $Wm^{-2}K^{-1}$			R/10^{-7} m^2KW^{-1}
							Sim.	Cal.	Ref.	
Al	/		70.0	2.7	0.3	27				
GFs	In-plane	300	1153	2.2	0.195	12		11	4.8	
	Out-of-plane		39.511	2.2	0.0002	12		130		
a							1.37			7.29
b							1.82			5.49
c							1.0			10
d							0.823			12.1

CHASPTER 4 CONCLUTION

Composites with varying volume fractions of GFs/Al (5vol%, 10vol%, 15vol%, and 20vol%) were fabricated using Spark Plasma Sintering (SPS). The microstructures of these composites were examined, and their relative density and Effective Thermal Conductivity (ETC) were measured. The measured ETC values for Samples a to d were 167.8, 169.6, 170.4, and 171.2 W m^{-1} K^{-1}, respectively. These values were found to be lower than the ETCs calculated using the Rule of Mixtures (ROM), which were 185.73, 218.33, 254.62, and 288.96 W m^{-1} K^{-1} for Samples a to d, respectively.

The average angles between the GFs and the heat flow direction were determined as follows: 18.6° for Sample a, 16.3° for Sample b, 14.6° for Sample c, and 14.1° for Sample d. The ETCs of the composites, considering the orientations of the GFs, were evaluated using a 2D image-based simulation. The impact of interfacial thermal resistance on ETCs was assessed by comparing the simulation results with the measured ETC values. As a result, ETCs decreased by 9.6%, 22.3%, 33.3%, and 40.6% for Samples a to d, respectively, due to the presence of interfacial thermal resistance.The thermal resistance (R) at the Al/GF interface was determined to be 7.29×10^{-7}, 5.49×10^{-7}, 10×10^{-7}, and 12.15×10^{-7} W m^{-2} K^{-1} for Samples, respectively.

REFERENCES

[1] Chung D. Properties of Carbon Fibers, Carbon Fiber Composites. Butterworth Heinemann, Newton 1994.

[2] Huang Y, Ouyang Q, Guo Q, Guo X, Zhang G, Zhang D. Graphite film/aluminum laminate composites with ultrahigh thermal conductivity for thermal management applications. Materials & Design. 2016; 90:508-15.

[3] Chen JK, Huang IS. Thermal properties of aluminum–graphite composites by powder metallurgy. Composites Part B: Engineering. 2013;44(1):698-703.

[4] Li W, Liu Y, Wu G. Preparation of graphite flakes/Al with preferred orientation and high thermal conductivity by squeeze casting. Carbon. 2015; 95:545-51.

[5] K. Sugio, Y.-B. Choi and G. Sasaki: Mater. Trans. 57 (2016) 582-589.

[6] Zhou C, Ji G, Chen Z, Wang M, Addad A, Schryvers D, et al. Fabrication, interface characterization and modeling of oriented graphite flakes/Si/Al composites for thermal management applications. Materials & Design. 2014; 63:719-28.

[7] Kidalov S, Shakhov F. Thermal Conductivity of Diamond Composites. Materials. 2009;2(4):2467-95.

[8] Xue C, Bai H, Tao PF, Wang JW, Jiang N, Wang SL. Thermal conductivity and mechanical properties of flake graphite/Al composite with a SiC nano layer on graphite surface. Materials & Design. 2016; 108:250-8

[9] Kurita H, Miyazaki T, Kawasaki A, Lu Y, Silvain J-F. Interfacial microstructure of graphite flake reinforced aluminum matrix composites fabricated via hot pressing. Composites Part A: Applied Science and Manufacturing. 2015; 73:125-31.

[10] Zhou C, Chen D, Zhang XB, Chen Z, Zhong SY, Wu Y, et al. The roles of geometry and topology structures of graphite fillers on thermal conductivity of the graphite/aluminum composites. Physics Letters A. 2015;379(5):452-7.

[11] Chang J, Zhang Q, Lin Y, Wu G. Layer by layer graphite film reinforced aluminum composites with an enhanced performance of thermal conduction in the thermal management applications. Journal of Alloys and Compounds. 2018;742:601-9.

[12] KURAMOTO H, MATSUGI K, KAWAHARAK, YANAGISAWA O. Densification rate of Cu-Al2O3 composite in the spark sintering process. Nippon Kinzoku Gakkaishi (1952). 2003;67(10):528-37

[13] KERNER EH. The Elastic and Thermo-elastic Properties of Composite Media. Proc Phys Soc Sec B. 1956;69(8):808-13.

[14] Schapery RA. Thermal Expansion Coefficients of Composite Materials Based on Energy Principles. Journal of Composite Materials. 1968;2(3):380-404.

[15] Xue C, Bai H, Tao PF, Jiang N, Wang SL. Analysis on Thermal Conductivity of Graphite/Al Composite by Experimental and Modeling Study. Journal of Materials Engineering and Performance. 2016;26(1):327-34.

[16]Sugio K, Tatsuno S, Fukushima H, Yanagisawa O. Modification of KolmogorovJohnson-Mehl-Avrami Equation for Clustered Nucleation. Materials Transactions.2009;50(6):1563-71.

[17] Cho J, Luo J, Daniel I. Mechanical characterization of graphite/epoxy nanocomposites by multi-scale analysis. Composites science and technology. 2007;67(11-12):2399-407.

ACKNOWLEDGEMENTS

This paper not only reflects my two years of study and research results, at the same time it also more condensed teachers, classmates, friends and support and help. I would like to express my heartfelt thanks to them.

My supervisor, Prof. Sugio, gave me comprehensive and detailed guidance for the completion of my thesis, from the selection of the topic, the formulation of the outline, the development of the research work until the completion of the thesis, Prof. Sugio's efforts were devoted. Although he was busy with his work, he often found time to provide me with guidance and support through interviews and e-mails. He helped me to solve the problems and difficulties that arose in my research, which made me take fewer detours in my daily work and study.

In addition, my classmates in the research laboratory provided me with great help from the beginning of the project to the completion of the dissertation, and they still ask me about my work, life, and the completion of the dissertation, and provide me with reasonable advice and suggestions based on their own practical experience. My classmates and Prof. Sasaki and Prof. Matsuki have also kept in touch with the progress of my dissertation and provided me with targeted advice and suggestions and have often reminded me that I should take my dissertation seriously, that I should not be sloppy at any time, and that I should be careful in revising it.

Finally, I would like to express my deepest gratitude to my teachers and classmates who have supported and taught me in my studies and life during the two years.